

TABLE OF CONTENTS

COMMUNICATIONS

Processing of submicron grain 304 stainless steel

M. Jain, T. Christman

Microstructures and electrical resistivities of the RuO₂ electrode on SiO₂/Si annealed in the oxygen ambient

J.S. Lee, H.J. Kwon, Y.W. Jeong, H.H. Kim, C.Y. Kim

Synthesis of bulk nanocrystalline Ti-Cu alloy by pressure-quenching method

D. Li, A. Wang, B. Yao, B. Ding, Z. Hu

The oxidation behavior and magnetic properties of iron carbonitride ultrafine particles

X.Q. Zhao, Y. Liang, Z.Q. Hu, B.X. Liu

ARTICLES

Effect of temperature gradient in the solution on spiral growth of YBa₂Cu₃O_{7-x} bulk single crystals

Y. Kanamori, Y. Shiohara

Preparation of YBa₂Cu₃O_{7-δ} thin film by laser-assisted metal organic chemical vapor deposition using highly volatile fluorocarbon-based Ba source

Y. Mizushima, I. Hirabayashi

The growth mechanism and morphology of melt-texture-growth processed YBa₂Cu₃O_{7-δ} with different pre-sintered microstructures

J. Wang, I. Monot, G. Desgardin

Influences of oxygen partial pressure on YBCO grain growth by a zone melting method

X. Yao, M. Sumida, Y. Shiohara

Thermal decomposition of mechanically alloyed nanocrystalline fcc Fe₆₀Cu₄₀

J.Y. Huang, Y.D. Yu, Y.K. Wu, H.Q. Ye, Z.F. Dong

Synthesis of submicrometer-grained-ultrahigh-carbon steel containing 10% aluminum by ball milling of powders

E.M. Taleff, M. Nagao, Y. Ashida, O.D. Sherby

Superplastic deformation characteristics and constitution equation in rapidly solidified Mg-Al-Ga alloy

A. Uoya, T. Shibata, K. Higashi, A. Inoue, T. Masumoto

Oxidation and crystallization of an amorphous Zr₆₀Al₁₅Ni₂₅ alloy

X. Sun, S. Schneider, U. Geyer, W.L. Johnson, M-A. Nicolet

Etching of polycrystalline diamond films by electron beam assisted plasma

K. Kobashi, S. Miyauchi, K. Miyata, K. Nishimura, J.J. Rocca

Tribological properties of fullerenes C₆₀ and C₇₀ microparticles

W. Zhao, J. Tang, A. Puri, R.L. Sweany, Y. Li, L. Chen

Thermodynamic stability of binary oxides in contact with silicon

K.J. Hubbard, D.G. Schlom

A novel mosaic-like structure in SrTiO₃ thin films on a Pt(001) surface revealed by transmission electron microscopy

S. Takeno, S. Nakamura, K. Abe, S. Komatsu

Anelastic and plastic relaxation in polycrystalline alumina and single-crystal sapphire

K. Ota, G. Pezzotti

Rare-earth-doped α¹-Sialon ceramics with novel optical properties

B.S.B. Karunaratne, R.J. Lumby, M.H. Lewis

Residual stress in ceramics with large thermal expansion anisotropy

S.W. Paulik, M.H. Zimmerman, K.T. Faber, E.R. Fuller Jr.

Ternary packing of SiC and diamond particles in ethanol

J-H. Lee, W.J. Lackey, J.F. Benzel

In-flight formation of carbon-site vacancies and subsequent nitridation in titanium carbide powders during induction plasma treatment: Part II.

Thermal plasma treatment of titanium carbide powders

T. Ishigaki, Y. Moriyoshi, T. Watanabe, A. Kanzawa

Microstructure and strain in electrodeposited Cu/Ni multilayers

D. Van Heerden, E. Zolotoyabko, D. Shechtman

Optical properties of nanosized gold particles

R.H. Doremus, P. Rao

Melting process of nanometer-sized In particles embedded in an Al matrix synthesized by ball milling

H.W. Sheng, J. Xu, L.G. Yu, X.K. Sun, Z.Q. Hu, K. Lu

Optical emission spectroscopy during the bias enhanced nucleation of diamond microcrystals by microwave plasma chemical vapor deposition process

H.C. Barshilia, B.R. Mehta, V.D. Vankar

JMR Abstracts provides a listing of preliminary titles and abstracts tentatively scheduled to appear in the corresponding issue of *Journal of Materials Research*. Copyright 1996 by the Materials Research Society. All rights reserved. Although every effort is taken to provide accurate contents here, late schedule changes in *Journal of Materials Research* may result in articles being rescheduled for later issues or in the addition of late articles to an issue that may not be shown here. The Materials Research Society regrets any inconvenience that may result from late schedule changes. ISSN: 1066-2375.

Copper (I) oxide powder generation by spray pyrolysis

D. Majumdar, T.A. Shefelbine, T.T. Kudas, H.D. Glicksman

Hydrothermal growth and characterization of NaLa(WO₄)₂ crystals

K. Byrappa, A. Jain

Energy losses of ions implanted in matter

J.H. Liang, K.Y. Liao

Reaction sintering of alumina-aluminide alloys (3A)

N. Claussen, D.E. Garcia, R. Janssen

Electrical properties of polyethylene highly filled with carbon

F.A. Modine, A.R. Duggal, D.N. Robinson, E.L. Churnetski, M. Bartkowiak, G.D. Mahan, L.M. Levinson

Hardness and adhesive properties of (Cr,Mo) oxycarbide films on stainless steel via vapor deposition

M-H. Lo, W-C.J. Wei

Hardness and toughness of exoskeleton material in the stone crab, *Menippe mercenaria*

C.A. Melnick, Z. Chen, J.J. Mecholsky Jr.

Characterization of hydrated silicate glass microballoons

H. Isobe, I. Tokunaga, N. Nagai, K. Kaneko

Principle of dynamic decompression and cooling for materials processing

R.E. Apfel, N. Qiu

Crystal growth and textured microstructures of 1,6-di(N-carbazoyl)-2,4 hexadiyne diacetylene

J. Liao, D.C. Martin

Ar⁺ ion irradiation in oxygen environment for improving wettability of polymethylmethacrylate

S-K. Koh, W-K. Choi, J-S. Cho, S-K. Song, Y-M. Kim, H-J. Jung

ABSTRACTS

COMMUNICATIONS

Processing of submicron grain 304 stainless steel

M. Jain, T. Christman

(California Institute of Technology)

A novel thermo-mechanical processing technique for the synthesis of bulk submicron grain (grain size \approx 200 nm) 304 stainless steel is reported. This ingot-metallurgical technique requires a total deformation of only 95% and the key steps to this processing technique involve: (1) formation of ultrafine dislocation cell structure, and (2) the conversion of dislocation cells into grains with medium to high misorientation by grain boundary sliding.

Order No.: JA611-001

© 1996 MRS

Microstructures and electrical resistivities of the RuO₂ electrode on SiO₂/Si annealed in the oxygen ambient

J.S. Lee, H.J. Kwon, Y.W. Jeong, H.H. Kim, C.Y. Kim

(LG Electronics Research Center)

The electrical resistivity property of RuO₂ thin films grown on the SiO₂/Si substrate by reactive dc sputtering was examined in terms of microstructure using x-ray diffraction and cross-sectional transmission electron microscopy. As the samples were annealed in the oxygen ambient over the temperature range 300–700°C, the resistivity decreased from 270 to 90 $\mu\Omega\text{cm}$ with increasing annealing temperature. When heat treatment was performed below 500°C, the strain which accumulated in the RuO₂ layer during deposition was released without significant increase in grain size. It is thought that below 500°C the improvement in the crystallinity plays an important role in the variation of the resistivity. Although a considerable amount of growth of RuO₂ grains was achieved, the columnar structure of the RuO₂ layer in the as-deposited sample remained unchanged even after annealing at 700°C. The resistivity improvement above 500°C was driven mainly by the grain boundary annihilation.

Order No.: JA611-002

© 1996 MRS

Synthesis of bulk nanocrystalline Ti-Cu alloy by pressure-quenching method

D. Li, A. Wang, B. Yao, B. Ding, Z. Hu

(Academia Sinica)

A new method is proposed to prepare bulk nanocrystalline alloys by quenching alloy melts under high pressure. Due to application of pressure

to solidification processes, nucleation rate is increased whereas growth rate of nuclei decreased with an increase in pressure, which makes it possible to obtain bulk ingots with nanometer-sized crystalline grains if appropriate pressure, temperature and cooling rate are selected. The as-pressure-quenched products are cylinder-like with a diameter about 4 mm and a height of several millimeters. This method can produce dense, free-porosity bulk nanocrystalline alloys with clean crystalline interfaces, promising use for experimental research and technological application.

Order No.: JA611-003

© 1996 MRS

The oxidation behavior and magnetic properties of iron carbonitride ultrafine particlesX.Q. Zhao⁺, Y. Liang⁺, Z.Q. Hu⁺, B.X. Liu^{*}*(* Tsinghua University, +Chinese Academy of Sciences)*

Iron nitride and iron carbonitride (ICN) ultrafine particles (20–80 nm in size) have been synthesized by laser induced pyrolysis of Fe(CO)₅-NH₃-C₂H₄ system. The oxidation behavior, surface morphologies and structural characteristics as well as magnetic properties of these particles were reported and discussed. It is found that the presence of very thin carbon coating (1–2 nm) on the ICN particles play an important role in preventing the oxidation of the particles. Accordingly, the ICN ultrafine particles exhibit higher saturation magnetization (142 emu/g) than the iron nitride ones (124 emu/g).

Order No.: JA611-004

© 1996 MRS

ARTICLES

Effect of temperature gradient in the solution on spiral growth of YBa₂Cu₃O_{7-x} bulk single crystals

Y. Kanamori, Y. Shiohara

(Superconductivity Research Laboratory-ISTEC)

The bulk single crystals of Y123 are required to clarify the superconductivity phenomena and develop electronic devices using unique superconductive properties. Only the solute rich liquid-crystal pulling method has succeeded in continuous growth of the Y123 single crystal. In this paper, we investigated the growth of Y123 single crystals under different temperature gradients in the solution in order to understand the growth mechanism of Y123. It was revealed that Y123 single crystals grow with a spiral growth mode which is in good agreement with the BCF theory.

Order No.: JA611-005

© 1996 MRS

Preparation of $\text{YBa}_2\text{Cu}_3\text{O}_{7-\delta}$ thin film by laser-assisted metal organic chemical vapor deposition using highly volatile fluorocarbon-based Ba source

Y. Mizushima, I. Hirabayashi

(Superconductivity Research Laboratory-ISTEC)

Superconducting oxide films of $\text{YBa}_2\text{Cu}_3\text{O}_{7-\delta}$ (YBCO) were produced on magnesia (MgO) single crystalline substrates (100) by laser-assisted metalorganic chemical vapor deposition. The highly volatile $\text{Ba}(\text{hfa})_2$ tetraglyme was used as a Ba source metalorganic material. Smoother surface YBCO film was obtained with KrF laser irradiation than without. However, KrF laser irradiation does not lower the temperature for formation of YBCO(123) phase. YBCO film prepared at 750°C on the MgO substrate showed $T_c(=0)$ of 69 K; that prepared with KrF laser irradiation 85 K. When water was added to the reaction chamber, barium fluoride was reduced and the YBCO formation was detected at a temperature of 650°C and higher. YBCO film prepared at the temperature of 700°C for 40 minutes without KrF laser irradiation behaves as a semiconductor, and one prepared with laser irradiation showed $T_c(0)$ of 78 K.

Order No.: JA611-006

© 1996 MRS

The growth mechanism and morphology of melt-texture-growth processed $\text{YBa}_2\text{Cu}_3\text{O}_{7-\delta}$ with different pre-sintered microstructures

J. Wang, I. Monot, G. Desgardin

(ISMRA/Université de CAEN)

This work deals with the influence of the starting Y-123 grain size on the growth mechanism and final microstructure of the melt-textured $\text{YBa}_2\text{Cu}_3\text{O}_{7-x}$ ceramics. Observations of the growth front morphology and stability for the different precursors using several decomposition temperatures could be correlated with the theoretical equations. It is found that the final 211 inclusion size increases as the starting 123 grain size increases. However using a small-grained 123 precursor disrupts the growth front and makes the control of grain alignment difficult. An appropriate morphology of the 123 precursor should be chosen prior to the MTG process in order to obtain the best properties.

Order No.: JA611-007

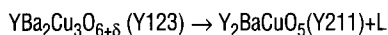
© 1996 MRS

Influences of oxygen partial pressure on YBCO grain growth by a zone melting method

X. Yao, M. Sumida, Y. Shiohara

(Superconductivity Research Laboratory-ISTEC)

This study reports investigation on influences of Y-Ba-Cu-O compounds solidification under different oxygen partial pressures by a zone melting method. In Y-Ba-Cu-O system, $P(\text{O}_2)$ ranged from 0.02 to 1 atm, the following reaction occurred during heating:



With an increase of oxygen partial pressure or decrease of pulling rate, the morphology of solidified interface changed from mushy to equiaxed, cellular and planar. The continuous Y123 grains were readily obtained under high oxygen partial pressure. Based on the constitutional supercooling theory and combining the result of the yttrium solubility limit for different oxygen partial pressures, the influences of oxygen partial pressure on Y123 morphological evolution were clarified.

Order No.: JA611-008

© 1996 MRS

Thermal decomposition of mechanically alloyed nanocrystalline fcc $\text{Fe}_{60}\text{Cu}_{40}$

J.Y. Huang, Y.D. Yu, Y.K. Wu, H.Q. Ye, Z.F. Dong

(Chinese Academy of Sciences)

A ferromagnetic and supersaturated fcc $\text{Fe}_{60}\text{Cu}_{40}$ solid solution has been prepared by mechanical alloying (MA). The phase transformations of the as-milled $\text{Fe}_{60}\text{Cu}_{40}$ powder upon heating to 1400°C and subsequently cooling to room temperature were characterized by differential thermal

analysis (DTA) and thermal magnetic measurement. The fcc $\text{Fe}_{60}\text{Cu}_{40}$ solid solution decomposes into $\alpha\text{-Fe}(\text{Cu}) + \gamma\text{-Fe}(\text{Cu}) + \text{Cu}(\text{Fe})$ upon heating from 300 to 460°C, and on the further heating, $\alpha\text{-Fe}(\text{Cu})$ transforms to $\gamma\text{-Fe}(\text{Cu})$ at 640→760°C; during cooling, the reverse transformation occurs from 800→640°C (obtained from thermomagnetic measurement) or from 700→622°C (obtained from DTA). The $\gamma \leftrightarrow \alpha$ transformation in mechanically alloyed $\text{Fe}_{60}\text{Cu}_{40}$ nanocrystalline occurs in a wide temperature range; and the transformation temperature is higher than that of the martensite transformation in as-cast Fe-Cu alloys, but is much lower than that of the allotropic transformation of pure Fe. These differences may be caused by the different fabrication processes, the non-equilibrium microstructure of MA as well as the inhomogeneous grain size in $\alpha\text{-Fe}(\text{Cu})$. High resolution transmission electron microscope (HRTEM) observations carried out in the specimen after DTA run shows that the N-W or K-S orientation relationships exist between $\alpha\text{-Fe}(\text{Cu})$ and $\text{Cu}(\text{Fe})$, which also represent the orientation relationship between $\alpha\text{-Fe}(\text{Cu})$ and $\gamma\text{-Fe}(\text{Cu})$ due to excellent coherency between $\gamma\text{-Fe}(\text{Cu})$ and $\text{Cu}(\text{Fe})$. The grain size of the $\alpha\text{-Fe}(\text{Cu})$ is inhomogeneous and varies from 50–600 nm. Energy dispersive x-ray spectroscopy (EDXS) results show that the Cu content in these $\alpha\text{-Fe}(\text{Cu})$ grains reaches as high as 9.5 at.% even after DTA heating to 1400°C, which is even higher than the maximum solubility of Cu in $\gamma\text{-Fe}$ above 1094°C. This may be caused by the small grain size of $\alpha\text{-Fe}(\text{Cu})$.

Order No.: JA611-009

© 1996 MRS

Synthesis of submicrometer-grained-ultrahigh-carbon steel containing 10% aluminum by ball milling of powders

E.M. Taleff*, M. Nagao*, Y. Ashida*, O.D. Sherby#

(* The University of Texas at Austin, *Kobe Steel, Ltd., #Stanford University)

An ultrahigh-carbon (1.25 wt.%) steel alloy containing 10 wt.% aluminum (UHCS-10Al) was processed by a powder metallurgy technique. Gas-atomized powders were subjected to ball milling in an attritor in order to obtain a submicrometer grain size. Powder material was consolidated by both hot isostatic pressing (HIP) and by hot isopressure extrusion (HIE). Bulk material with submicrometer grain sizes was produced from attrited powders. The chemical composition and microstructure of this material is characterized at each processing step, from atomization through consolidation. Tensile tests show that a high strength results from the submicrometer grain size produced in the bulk material.

Order No.: JA611-010

© 1996 MRS

Superplastic deformation characteristics and constitution equation in rapidly solidified Mg-Al-Ga alloy

A. Uoya*, T. Shibata*, K. Higashi*, A. Inoue#, T. Masumoto#

(* YKK Corporation, +University of Osaka Prefecture, #Tohoku University)

The hot deformation characteristics of a newly typed high strength magnesium-based alloy, Mg-8.3wt.%Al-8.1wt.%Ga alloy produced by rapidly solidified and powder metallurgy method have been investigated. Tensile tests were carried out at a temperature range from 523 to 623 K and a strain rate range from 10^{-4} to 1 s^{-1} . Superplastic characteristics were found and, especially, a maximum elongation-to-failure of 1080% was obtained at 573 K and at a relatively high strain rate of 10^{-2} s^{-1} . Because of the presence of fine microstructures at high temperatures, the optimum superplastic strain rate of the Mg-Al-Ga alloy was higher than that of the reported conventional superplastic aluminum and magnesium alloys.

Order No.: JA611-011

© 1996 MRS

Oxidation and crystallization of an amorphous $\text{Zr}_{60}\text{Al}_{15}\text{Ni}_{25}$ alloy

X. Sun, S. Schneider, U. Geyer, W.L. Johnson, M-A. Nicolet

(California Institute of Technology)

The amorphous ternary metallic alloy $\text{Zr}_{60}\text{Al}_{15}\text{Ni}_{25}$ was oxidized in dry oxygen in the temperature range 310°C to 410°C. Rutherford backscattering (RBS) and cross-sectional transmission electron microscopy studies (TEM) suggest that during this treatment an amorphous layer of zirconium-

aluminum-oxide is formed at the surface. Nickel was depleted in the oxide and enriched in the amorphous alloy near the interface. The oxide layer thickness grows parabolically with annealing duration, with a transport constant of $2.8 \times 10^{-5} \text{ m}^2/\text{s} \times \exp(-1.7 \text{ eV} / \text{KT})$. The oxidation rate may be controlled by the diffusion of Ni in the amorphous alloy.

At later stages of the oxidation process, precipitates of nanocrystalline ZrO_2 appear in the oxide near the interface. Finally, two intermetallic phases nucleate and grow simultaneously in the alloy, one at the interface and one within the alloy. An explanation involving preferential oxidation is proposed.

Order No.: JA611-012

© 1996 MRS

Etching of polycrystalline diamond films by electron beam assisted plasma

K. Kobashi*, S. Miyauchi*, K. Miyata*, K. Nishimura*, J.J. Rocca*
(*Kobe Steel, Ltd., +Colorado State University)

Polycrystalline diamond films were processed in a direct current plasma produced by a self-focused electron beam using combinations of H_2 , O_2 and He as the processing gas. The film surfaces were observed by scanning electron microscopy, and characterized by x-ray photoelectron spectroscopy. It was found that for the case that O_2 was included in the processing gas, a high density of etch pits appears on (100) faces of diamond grains, and oxygen was either physisorbed or chemisorbed at the film surface. It was demonstrated that the etching apparatus used was capable of forming at least a $5 \mu\text{m}$ wide pattern of polycrystalline diamond film.

Order No.: JA611-013

© 1996 MRS

Tribological properties of fullerenes C_{60} and C_{70} microparticles

W. Zhao*, J. Tang*, A. Puri*, R.L. Sweany*, Y. Li*, L. Chen*
(*University of New Orleans, +Chinese Academy of Sciences)

The frictional behaviors of fullerenes C_{60} and C_{70} were studied because they were speculated to be solid lubricants. For the sublimated pure C_{60} films on Si (001), a high friction coefficient (0.55–0.8) was observed under different loads and pin materials. For the C_{70} film, the friction coefficient showed a pin dependence, which changed from 0.5 with an Al_2O_3 pin to about 0.9 with a 440 stainless steel pin. The relatively high friction coefficients of C_{60} and C_{70} films were due to the tendency of the C_{60} and C_{70} particles to clump and compress into high shear strength layers rather than due to the impurities in the fullerenes. The benzene-solvated $\text{C}_{60}\cdot 4\text{C}_6\text{H}_6$ and $\text{C}_{70}\cdot x\text{C}_6\text{H}_6$ showed a lowered friction coefficient (0.25 for $\text{C}_{60}\cdot 4\text{C}_6\text{H}_6$ and 0.3 for $\text{C}_{70}\cdot x\text{C}_6\text{H}_6$), which might result from the lowered shear strength of the hcp structure of $\text{C}_{60}\cdot 4\text{C}_6\text{H}_6$ and $\text{C}_{70}\cdot x\text{C}_6\text{H}_6$ molecular crystals in which the benzene molecules were intercalated.

Order No.: JA611-014

© 1996 MRS

Thermodynamic stability of binary oxides in contact with silicon

K.J. Hubbard, D.G. Schlom

(The Pennsylvania State University)

Using tabulated thermodynamic data, a comprehensive investigation of the thermodynamic stability of binary oxides in contact with silicon at 1000 K was conducted. Reactions between silicon and each binary oxide at 1000 K, including those involving ternary phases, were considered. Sufficient data exists to conclude that all binary oxides except the following are thermodynamically unstable in contact with silicon at 1000 K: Li_2O , most of the alkaline earth oxides (BeO, MgO, CaO, and SrO), the column IIIB oxides (Sc_2O_3 , Y_2O_3 , and Re_2O_3 where Re is a rare earth), ThO_2 , UO_2 , ZrO_2 , HfO_2 , and Al_2O_3 . Of these remaining oxides, sufficient data exists to conclude that BeO, MgO, and ZrO_2 are thermodynamically stable in contact with silicon at 1000 K. Our results are consistent with reported investigations of silicon/binary oxide interfaces and identify candidate materials for future investigations.

Order No.: JA611-015

© 1996 MRS

A novel mosaic-like structure in SrTiO_3 thin films on a Pt(001) surface revealed by transmission electron microscopy

S. Takeno, S. Nakamura, K. Abe, S. Komatsu
(Toshiba Corp.)

A novel mosaic-like structure in SrTiO_3 thin films was discovered and characterized by means of transmission electron microscopy (TEM). The films were deposited on a (001) oriented Pt surface. The orientation relationship between SrTiO_3 film and Pt substrate was determined and four types of growth modes were revealed. These four growth modes formed four types of domains, respectively, and these domains and Pt formed peculiarly ordered interfacial structures, i.e., near coincidence site lattices. Anti-phase boundaries between two adjacent domains were also observed by high-resolution imaging.

Order No.: JA611-016

© 1996 MRS

Anelastic and plastic relaxation in polycrystalline alumina and single-crystal sapphire

K. Ota*, G. Pezzotti*

(*Osaka University, +Toyoashi University of Technology)

Internal friction and torsional creep behaviors of high-purity single-crystal sapphire and three polycrystalline aluminas with different grain sizes have been measured up to a very high temperature. The hexagonal c-axis-oriented sapphire specimen was tested at frequencies of 10–13 Hz, up to melting point (i.e., ~2323 K). No relaxation peak was found and the exponential background curve was discussed in analogy to that of the hexagonal single-crystal ice reported in previous literature. The internal friction curves of the polycrystalline specimens were constituted by the superposition of a background component, of plastic nature, and a broad anelastic grain-boundary peak. These curves were markedly shifted to lower temperatures as compared to that of sapphire; the higher the shift, the smaller the average grain size. Also, the intensity of grain-boundary peak decreased when increasing the grain size. In the polycrystalline specimens, both creep and internal-friction background data were fitting the same Arrhenius plot, the slope corresponding to an activation energy of 200 kJ/mol. These data provide evidence for the occurrence of anelastic relaxation at the grain boundary and for the plastic nature of the internal-friction background in Al_2O_3 ceramics.

Order No.: JA611-017

© 1996 MRS

Rare-earth-doped α' -Sialon ceramics with novel optical properties

B.S.B. Karunaratne, R.J. Lumby, M.H. Lewis

(University of Warwick)

A totally new phenomenon has been observed in the field of Sialon ceramics which may lead to applications based on their optical or electronic properties in addition to their excellent mechanical and thermal properties. For the first time a colored α' -Sialon ceramic with relatively high optical transparency has been produced by careful control of the sintering atmosphere, and adding suitable rare earths in an appropriate valence state as stabilizing cations. This compares with normal Sialons and silicon nitrides which are grey-black in color and are opaque.

Order No.: JA611-018

© 1996 MRS

Residual stress in ceramics with large thermal expansion anisotropy

S.W. Paulik*, M.H. Zimmerman*, K.T. Faber*, E.R. Fuller Jr.*

(*Northwestern University, +National Institute of Standards and Technology)

Residual stress was measured in sintered and heat-treated Fe_2TiO_5 samples with various grain sizes. The influence of texturing was assessed by comparing the residual stress states of samples having randomly-oriented grains and highly-oriented grains produced through magnetically-assisted processing. The residual stress was measured with x-ray diffraction using $\text{Cr K}\alpha$ radiation. Due to the significant texture and the consequential oscillations in the $d_{\psi\psi}$ vs. $\sin^2\psi$ data, the residual stress was calculated using the Marion-Cohen method. Textured samples showed

significantly lower residual stresses except when spontaneous microcracking accompanied grain growth in the randomly-oriented systems. Elastic modulus measurements showed a direct correlation between the decrease in residual stress and the microcrack density.

Order No.: JA611-019

© 1996 MRS

Ternary packing of SiC and diamond particles in ethanol

J.-H. Lee, W.J. Lackey, J.F. Benzel
(Georgia Institute of Technology)

Particle packing techniques employing a liquid phase were used for preparation of dense disks of SiC and diamond particulates. Forty-one SiC and fifteen diamond compositions in the ternary-component particle systems were used to determine the optimum percentages of coarse, medium, and fine particles for achieving high packing densities; over 80% for SiC and over 62% for diamond. High packing densities were achieved without vibration by simply mixing the three size fractions in ethanol followed by stirring during the initial evaporation stage. The packing density results for SiC were successfully correlated with the percentages of the coarse and fine particles using multiple regression analysis; however, the data for diamond could not be similarly correlated with particle composition because the experimental work was done in a narrow range of compositions and the range of packing densities was small.

Order No.: JA611-020

© 1996 MRS

In-flight formation of carbon-site vacancies and subsequent nitridation in titanium carbide powders during induction plasma treatment: Part II. Thermal plasma treatment of titanium carbide powders

T. Ishigaki*, Y. Moriyoshi*, T. Watanabe*, A. Kanzawa*
(* National Institute for Research in Inorganic Materials, + Tokyo Institute of Technology)

The in-flight modification of titanium carbide powders was carried out in R.F. inductively coupled plasmas. The powders were partially melted and evaporated, and then subjected to modifications in morphology, size and chemical composition. Both the Ar-H₂ and Ar-N₂ plasma treatments induced the formation of carbon-site vacancies in titanium carbide. The mixing of NH₃ to Ar-H₂ plasma at the plasma tail, and the Ar-N₂ plasma treatment resulted in the partial substitution of carbon by nitrogen. The variation in physical and chemical modification was discussed compared with the predictions by the thermochemical analysis, and the numerically obtained heat transfer in our preceding paper.

Order No.: JA611-021

© 1996 MRS

Microstructure and strain in electrodeposited Cu/Ni multilayers

D. Van Heerden*, E. Zolotoyabko*, D. Shechtman*
(* National Institute of Standards and Technology, + Technion-Israel Institute of Technology)

Electrodeposited Cu/Ni multilayers with different modulation lengths $\Lambda=4-18$ nm were examined by means of x-ray diffraction and transmission electron microscopy. Preferred orientations of [111], [110] and [001]-types, as determined from relative x-ray diffraction peak intensities, were seen in the multilayers. By means of computer simulations of the measured x-ray diffraction spectra several parameters of the multilayers, such as Λ -values and fluctuations $\Delta\Lambda$ as well as lattice strain, were determined. Multilayers having large Λ were found to be fully relaxed due to interfacial dislocation formation. In short Λ [001]-textured multilayers partial strain relaxation occurs, probably due to the incorporation of Cu into the Ni layers. Both of the processes lead to the diffuse Cu/Ni interfaces. Short wavelength multilayers with a [111]-preferred orientation were almost fully strained. The importance of the [111]-texture in the improvement of mechanical strength of Cu/Ni multilayers resulting from its enhanced ability for strain accommodation is discussed.

Order No.: JA611-022

© 1996 MRS

Optical properties of nanosized gold particles

R.H. Doremus, P. Rao
(Rensselaer Polytechnic Institute)

Gold particles smaller than 2 nm in diameter were grown in glass. Their optical absorption spectrum did not show the usual plasma absorption band for gold particles; this band was spread by the small particle size. The absorption spectrum was calculated from the bulk optical properties of gold, modified for the small particle size; there was good agreement between calculated and measured spectra. The smallest particles containing from 20 to 40 gold atoms showed a λ^{-4} dependence of absorption on wave length λ . This result implies that the absorption in these particles was entirely from free electrons at wave lengths above 0.3 μm .

Order No.: JA611-023

© 1996 MRS

Melting process of nanometer-sized In particles embedded in an Al matrix synthesized by ball milling

H.W. Sheng, J. Xu, L.G. Yu, X.K. Sun, Z.Q. Hu, K. Lu
(Chinese Academy of Sciences)

Dispersions of nanometer-sized In particles embedded in an Al matrix (10 wt.% In) have been synthesized by ball milling of a mixture of Al and In powders. The as-milled product was characterized by using x-ray diffraction (XRD), scanning electron microscopy (SEM), energy dispersive x-ray spectrometer (EDX), transmission electron microscopy (TEM) and high resolution transmission electron microscopy (HREM), respectively. It was found that In and Al are pure components immiscible with each other, with nanometer-sized In particles dispersively embedded in the Al matrix. The melting behavior of In particles was investigated by means of differential scanning calorimeter (DSC). The calorimetric measurements indicate that both the melting point and the melting enthalpy of the In nanoparticles decrease with increasing milling time, or refinement of the In particles. Compared to its bulk melting temperature, a melting point depression of 13.4 K was observed when the mean grain size of In is 15 nm, and the melting point depression of In nanoparticles is proportional to the reciprocal of the mean grain size. The melting enthalpy depression was interpreted according to the two-state concept for the nanoparticles. Melting of the interface was deduced to be an exothermal process due to its large excess energy/volume.

Order No.: JA611-024

© 1996 MRS

Optical emission spectroscopy during the bias enhanced nucleation of diamond microcrystals by microwave plasma chemical vapor deposition process

H.C. Barshilia, B.R. Mehta, V.D. Vankar
(Indian Institute of Technology)

Microwave plasma chemical vapor deposition (MWPCVD) process has been used to grow diamond thin films on silicon substrates from CH₄-H₂ gas mixture. Bias enhanced nucleation (BEN) pretreatment has been used to increase the density of diamond nuclei. Various species in the CH₄-H₂ plasma have been identified using optical emission spectroscopy (OES) and their effect on the film microstructure has been studied. During pretreatment process the emission intensities of CH, CH⁺, C₂, H and H₂ species have been found to increase significantly for a negative dc bias voltage $|V_B| > 60$ V. The higher concentration of excited species and the associated effects play a significant role in the growth process. A very thin layer of a-C containing predominant sp³ bonded carbon species in the initial stages of the growth is found to be present in these films. The microstructure of the films has been found to be very sensitive to the biasing conditions.

Order No.: JA611-025

© 1996 MRS

Copper (I) oxide powder generation by spray pyrolysis

D. Majumdar*, T.A. Shefelbine*, T.T. Kodas*, H.D. Glicksman*
(*University of New Mexico, +DuPont Company)

Copper oxide powders were prepared by the spray pyrolysis of copper nitrate solutions over a range of temperatures (400–1300°C) and residence times (3–7 s). Phase-pure (by x-ray diffraction (XRD)) copper (I) oxide was obtained at 800–1300°C in an inert (nitrogen) atmosphere. The particles varied from smooth, solid spheres at 1300°C to irregularly shaped and hollow particles at 800°C with dense particles of Cu₂O being made only at 1000°C or higher. The particles were polycrystalline with an average crystallite size of 42 nm at 800°C while at 1000–1200°C, the particles were single crystals. Spray-pyrolysis in forming gas (7%H₂-N₂) atmosphere at 500–700°C gave Cu while spray-pyrolysis in air yielded CuO over 800–1000°C and a mixture of Cu₂O/CuO at 1200°C. These results show that solid, phase-pure Cu₂O particles can be produced by aerosol-phase densification at temperatures below its melting point (1235°C).

Order No.: JA611-026

© 1996 MRS

Hydrothermal growth and characterization of NaLa(WO₄)₂ crystals

K. Byrappa, A. Jain
(Mysore University)

The growth of NaLa(WO₄)₂ crystals has been carried out by hydrothermal method at fairly lower PT conditions. The crystal morphology has been studied with respect to the growth parameters. The crystals obtained were characterized by various techniques like XRD, DTA and IR spectroscopy.

Order No.: JA611-027

© 1996 MRS

Energy losses of ions implanted in matter

J.H. Liang, K.Y. Liao
(National Tsing Hua University)

A set of simple and accurate formulae for the first four moments of nuclear and electronic energy losses is proposed. A new variable is introduced to include the finite maximum-impact-parameter effect in the nuclear stopping process, which is assumed to be infinite in most studies. A critical energy at which the electronic energy loss is equal to the nuclear energy loss is also defined. It determines whether the nuclear or the electronic stopping process is the dominant mechanism in terms of incident-ion energy. The critical energy increases for heavy ions implanted in heavy target materials during the first moment of energy loss. The second moment of electronic energy loss is important only for light ions implanted at high ion energies. The third and fourth moments of nuclear energy loss are much larger than those of the electronic energy loss for all ion-target combinations. Theoretical predictions of the projected ranges and range stragglings for gold ions implanted in carbon films are close to the experimental data when these proposed four moments of nuclear and electronic energy losses are considered.

Order No.: JA611-028

© 1996 MRS

Reaction sintering of alumina-aluminide alloys (3A)

N. Claussen, D.E. García, R. Janssen
(Technische Universität Hamburg-Harburg)

A novel pressureless reaction sintering process is presented for the fabrication of Al₂O₃-aluminide alloys (3A). Compacts of intensively milled metal oxide-aluminium mixtures are heat-treated in vacuum or inert atmospheres such that the exothermic reactions take place in a controlled manner essentially at temperatures below the melting point of Al. Dense homogeneous microstructures were obtained with a variety of Al₂O₃-matrix systems with interpenetrating networks of aluminides of Ti, Fe, Nb, Mo, Zr, Ni, etc. By adding modifiers in the form of oxides or metals, volume and phase composition as well as properties can be tailored in a wide range.

Order No.: JA611-029

© 1996 MRS

Electrical properties of polyethylene highly filled with carbon

F.A. Modine*, A.R. Duggal*, D.N. Robinson#, E.L. Churnetski#, M. Bartkowiak*, G.D. Mahan***, L.M. Levinson+
(*Oak Ridge National Laboratory, +General Electric Co., #Oak Ridge Y-12 Plant, **University of Tennessee)

Carbon-filled polyethylene composites were fabricated and tested to establish the practical lower limit of their electrical resistivity at room temperature and to investigate the trade-offs between low resistivity and the magnitude of the resistance anomaly (i.e., a large positive temperature coefficient of resistivity) that appears when such composites are heated through the polyethylene crystalline melting transition. Carbon blacks with large particle size and low surface area provided low-resistivity composites having large resistance anomalies. The largest resistance anomalies were found in composites that were well mixed, but the room-temperature resistivity also increased in well-mixed materials. The size of the resistance anomaly increased in composites that were cycled repetitively through the crystalline-melting transition. A mixture of carbon blacks of two different sizes provided a lower resistance than was found in a material with the same fill of only the coarser black. By controlling the composition and the processing, composites were made with room-temperature resistivities lower than 0.2 ohm cm and resistance changes of at least 2 orders of magnitude. A resistance change of as much as 5 orders of magnitude was obtained for composites with room-temperature resistivities of only 1 ohm cm.

Order No.: JA611-030

© 1996 MRS

Hardness and adhesive properties of (Cr,Mo) oxycarbide films on stainless steel via vapor deposition

M-H. Lo, W-C.J. Wei
(National Taiwan University)

A hexacarbonyl of chromium and molybdenum ((Cr,Mo)(CO)₆) was used as an oxycarbide source for the coating on stainless steel 304 (SS304) at temperatures varied from 175°C to 450°C. Hardness of the films was determined from a microindentation technique through a similar calculation after Thomas [1987]. Intrinsic hardnesses of the films formed at low and medium temperatures were determined to be 8.61 and 2.75 GPa, respectively. Both of them are larger than that of SS304 substrate, 1.75 GPa. Adhesive strength of the films were measured by scratching test. The results reveal that the adhesive strength of the films formed at low, medium and high temperatures are 2.8 N, 37.6 N, and 36.0 N, respectively. Two different fracture modes after scratching were found for the films obtained at various temperature regions. A spalling-off type or a deformation failure with many cracks and deformation bands beside the striation were found.

Order No.: JA611-031

© 1996 MRS

Hardness and toughness of exoskeleton material in the stone crab, *Menippe mercenaria*

C.A. Melnick, Z. Chen, J.J. Mecholsky Jr.
(University of Florida)

Techniques from the field of materials science and engineering were utilized to examine the mechanical effects of dark pigment in exoskeleton material on the distal portion of stone crab, *Menippe mercenaria* chelae. We made specimens from dark and light colored exoskeleton material to measure hardness and fracture toughness. The results from these tests showed the dark material to be much harder and tougher than light colored material from the same crab chela. Scanning electron microscope photographs are presented to document the microstructure and level of porosity. We think that the structural difference in material properties is due to the lower level of porosity and phenolic tanning in dark material and that this tanning caused the dark color and filling of porosity. The exoskeleton structure is a laminated organic-inorganic structure which can serve as a model for self-healing structures.

Order No.: JA611-032

© 1996 MRS

Characterization of hydrated silicate glass microballoons

H. Isobe*, I. Tokunaga+, N. Nagai+, K. Kaneko+
 (*Fuji Chemical Co., Ltd., +Chiba University)

Glass microballoons (GB) of about 1 μm in diameter were prepared by ultrasonic spray pyrolysis from sodium silicate solution. Silica rich type of glass microballoons (SB) were prepared by acid treatment of GB. The structural changes of both microballoons with thermal treatment up to 973 K were examined. Both GB and SB showed properties similar to hydrated sodium silicate glass to some extent. SB was more thermally stable than GB, but the spherical structures of both microballoons were collapsed by heating at 973 K; cristobalite was observed in samples heated at 973 K. The loosely and tightly incorporated water molecules were evolved up to 573 K and near 850 K, respectively. The crystallization of cristobalite caused the tightly incorporated water molecules to evolve. The ultramicropores accessible only to H_2O molecules in SB gradually decreased by heating and disappeared by heating at 773 K.

Order No.: JA611-033

© 1996 MRS

Principle of dynamic decompression and cooling for materials processing

R.E. Apfel, N. Qiu
 (Yale University)

When a melt seeded with droplets of a volatile liquid is rapidly decompressed, the droplets explosively vaporize, taking their latent heat of vaporization from the melt and, therefore, homogeneously cooling and expanding it. The possibility of using this dynamic decompression and cooling (DDC) technique for producing an amorphous metallic foam is theoretically investigated. To test the premises of this theoretical model, preliminary experiments with an organic melt (*p*-terphenyl) seeded with water drops were performed. Results of these experiments demonstrate the potential of this novel approach to materials processing.

Order No.: JA611-034

© 1996 MRS

Crystal growth and textured microstructure of 1,6-di(N-carbazoyl)-2,4 hexadiyne diacetylene

J. Liao, D.C. Martin
 (The University of Michigan)

We are developing techniques to isolate and characterize grain boundary defects with controlled geometries in 1,6-di(N-carbazoyl)-2,4 hexadiyne (DCHD) diacetylene polymer bicrystals. To be successful in this endeavor, it is important to determine the influence of processing variables

such as evaporation rate, solution concentration, and environment on DCHD diacetylene crystal morphology. We have found that large, high quality DCHD diacetylene single crystals can be grown from solution under a controlled atmosphere. The quality of the DCHD crystals can be evaluated by optical microscopy and quantitative digital image analysis. Defect structures in DCHD diacetylene crystals have been studied by transmission electron microscopy (TEM). Two single-crystal textured structures have been found in porous DCHD crystals precipitated from solution: (1) a microfibrillar structure, and (2) a "cross-hatched" structure. The porous DCHD crystals show localized shear deformation zones (twins and kinks), but only in those regions where the density is greater than 95% that of the perfect crystal. Lateral chain invariant (LCI) small angle grain boundaries have been identified in DCHD by HREM.

Order No.: JA611-035

© 1996 MRS

Ar⁺ ion irradiation in oxygen environment for improving wettability of polymethylmethacrylate

S-K. Koh, W-K. Choi, J-S. Cho, S-K. Song, Y-M. Kim, H-J. Jung
 (Korea Institute of Science and Technology)

Ion irradiation with various oxygen flow rates has been carried out to improve the wettability of polymethylmethacrylate (PMMA) to water and to enhance the adhesion between Al and the polymer. Ar⁺ ion and oxygen ion were irradiated on the polymer, and amounts of ions were changed from 5×10^{14} Ar⁺/cm² to 5×10^{16} Ar⁺/cm² by a broad ion beam source. Oxygen gas from 0 ml/min. to 7 ml/min. was flowed near the polymer surface during the ion irradiation, and the energy of ions was changed from 500 eV to 1500 eV. Wetting angle was reduced from 68 degrees to 49 degrees with the Ar⁺ ion irradiation only at 1 keV energy, to 43 degrees with the oxygen ion irradiation, and dropped to 8 degrees with Ar⁺ ion irradiation with flowing 4 ml/min. oxygen gas near the polymer surface. Changes of wetting angle with oxygen gas and Ar⁺ ion irradiation were explained by a two-step chemical reaction among the polymer matrix, energetic ions and oxygen gas. Effects of Ar⁺ ion and oxygen ion irradiation were explained in a view of formation of hydrophilic groups due to a reaction between irradiated polymer chain by energetic ion irradiation and blown oxygen gas, and enhanced adhesion between Al and PMMA was explained by the formation of electron acceptor groups in polymer and electron donors in metal, and by the chemical reaction in the interface between irradiated polymer surface and deposited metal.

Order No.: JA611-036

© 1996 MRS

Please use the convenient postcard located in the back of the *MRS Bulletin* to order *JMR* reprints. When ordering single article reprints please note they are not available until the issue is published.
 See *JMR* Abstracts on the MRS Homepage at
<http://www.mrs.org/publications/jmr/jmra/>

Visit the Materials Research Society Homepage:
<http://www.mrs.org/>
 to keep up-to-date on MRS Meetings, Publications,
 and Membership News